Microsyst Technol (2011) 17:1283–1291
DOI 10.1007/s00542-011-1314-y

TECHNICAL PAPER

Digitally-controlled array of solid-state microcoolers for use in surgery

J. P. Carmo · M. F. Silva · J. F. Ribeiro · R. F. Wolffenbuttel · P. Alpuim · J. G. Rocha · L. M. Gonçalves · J. H. Correia

Received: 7 October 2010 / Accepted: 31 May 2011 / Published online: 14 June 2011

Abstract This paper presents an approach for generating a well-defined cooling pattern over an area of tissue. An array of solid-state microcoolers is used, which could be included in a probe that provides local cooling. This medical instrument can be used for removal of scar tissue in the eye or for the rapid stopping of bleeding due to micro-cuts, which makes it a useful tool to medical doctors and could make surgery more secure to the patient. The array of microcoolers is composed of 64 independent thermo-electric elements, each controlled using an integrated circuit designed in CMOS. The independent control allows the flexible programming of the surface temperature profile. This type of control is very suitable in case abrupt temperature steps should be avoided. Cooling by lateral heat flow was selected in order to minimize the influence of heat by dissipation from the electronic circuits. Moreover, a thermo-electric component with lateral heat allows fabrication of the cooling elements using planar thin-film technology, lithography and wet etching on top of the silicon wafer. This approach is potentially CMOS compatible, which would allow for the fabrication of the thermo-electric elements on top of a pre-fabricated CMOS wafer as a post-process step. Each pixel is composed of thin-films of n-type bismuth telluride, Bi_2Te_3 and p-type antimony telluride, Sb_2Te_3, which are electrically interconnected as thermocouple. These materials have excellent thermoelectric characteristics, such as thermoelectric figures-of-merit, *ZT*, at room temperatures of 0.84 and 0.5, respectively, which is equivalent to power-factors, *PF*, of 3.62×10^{-3} W K^{-1} m^{-2} and 2.81×10^{-3} W K^{-1} m^{-2}, respectively. The theoretical study presented here demonstrates a cooling capability of 15°C at room temperature (300 K ≈ 27°C). This cooling performance is sufficient to maintain a local tissue temperature at 25°C, which makes it suitable for the intended application. A first prototype was successfully fabricated to demonstrate the concept.

J. P. Carmo (✉) · M. F. Silva · J. F. Ribeiro · J. G. Rocha · L. M. Gonçalves · J. H. Correia
Department of Industrial Electronics, University of Minho, Campus Azurem, 4800-058 Guimaraes, Portugal
e-mail: jcarmo@dei.uminho.pt

P. Alpuim
Department of Physics, University of Minho, Campus Azurem, 4800-058 Guimaraes, Portugal

R. F. Wolffenbuttel
Department of ME/EI, Faculty of EEMCS, Delft University of Technology, Mekelweg 4, 2628CD Delft, The Netherlands

1 Introduction

Selective cooling of biological tissue has found several applications in medicine (Lewis and Mackenzie 1971; Treasure et al. 1988; Argonne National Laboratory 1006; Cheung et al. 1988; Larin et al. 2002; Davidson and Sherar 2003; Altshuler et al. 1999; Anvari et al. 1995). A promising new approach based on cooling of organs using an specially engineered ice slurry has been developed for patient treatment after a stroke and cardiac arrest by researchers at the University of Chicago (Argonne National Laboratory 2006). Basically, the idea is to rapidly cool the blood of targeted organs with a highly fluid mixture of small, smooth ice particles suspended in saline solution. Quickly lowering organ temperature by 4–10°C below the normal 37°C introduces cell protective hypothermia, which greatly reduces cell death. Also, in case of a sudden stroke or heart attack, rapid blood cooling could delay the death of heart and brain cells, giving doctors and paramedics more

time to revive victims. It is well demonstrated by these researchers that the ice slurry technology could also give surgeons more time to perform minimally invasive laparoscopic surgery, which frequently requires temporarily stopping blood flow to organs, such as kidneys or the liver. Cooling these organs before stopping their blood supply would give surgeons more time to operate before organ cells death is initiated by lack of oxygen (Argonne National Laboratory 2006).

Local cooling of biological tissues has also been used for treatment of cancer and benign tumors, muscle spasms, injuries and burns is another application that have been used for a long time (Larin et al. 2002). Cooling and freezing of tissues are employed not only in cryotherapy, but also in cryobiology for preserving organs, tissue and other biological objects. Real-time monitoring (and control) of cooling and freezing of tissues with a high spatial and time resolution is necessary for freezing biological objects to the required temperature at a cooling rate that makes it possible to preserve their normal structure and functioning (Larin et al. 2002). Cooling systems also found applications in urology, where urethral cooling catheters are used to prevent thermal damage to the urethra during thermal therapy of the prostate (Davidson and Sherar 2003). Once again, systems to control the temperature are needed to perform the quantification of a catheter's heat transfer for prediction of the catheter's influence on the temperature and thermal dose distribution in periurethral tissue (Davidson and Sherar 2003). Dermatology is another application of cooling systems, e.g., in medical procedures when skin pre-cooling helps to reduce epidermal thermal damage in laser procedures (such as hair removal) where the target structures are located up to several millimeters below the skin surface (Altshuler et al. 1999). The simultaneous use of lasers and cooling in these applications necessitates some kind of control. This means that the ability to control the position, degree and relative spatial distribution of cooling in biological tissues during a thermally mediated therapeutic procedure would be useful to medical doctors (Anvari et al. 1995). Local cooling is also used in eye surgery to remove excess scar tissue. A wide variety of cryogenic probes is available for scleral buckling and for treating retinal tears and detachments (DORC 2011). However, present systems are based on cryogenic nitreous oxide or carbon-dioxide gas fed to a probe using a tube. The solid-state probe would highly improve probe handling and would reduce eye damage during treatment caused by ice particles in the gas. Finally, it must be noted that there is sufficient evidence that therapeutic hypothermia after non-traumatic cardiac arrest improves neurological outcome and reduces mortality (Haugk et al. 2007).

The focus of this paper is the presentation of a digitally-controlled array of solid-state microcoolers for use in medical instruments to help medical doctors in surgeries. A possible application for this array is in cooling tips for use in microsurgery to locally cool the tissue in order to stop the bleeding, thus, reducing the risk of complications during surgery. In this type application the inner area of the surface covered by the cooling probe should not be cooled, while the outer edge should be at the lowest temperature. Moreover, these biomedical applications require: safety of operation, ease of manipulation, biocompatibility and low-levels of toxicity for patients. The solid-state microcooler array presented in this paper is intended to be especially suitable for meeting these requirements. Moreover, the compatibility with microelectronic circuit fabrication brings the objective of low unit price in mass production using batch processing of silicon wafers within reach.

2 Thermoelectric microconverters fabrication technology for microcoolers

Thermoelectric materials are solid-state energy converters whose combination of thermal, electrical, and semiconducting properties allows them to be used to convert waste heat into electricity. Alternatively, the effect is used to convert electrical power directly into cooling (Bell 2008). Thermoelectric devices based on these effects could form a new generation of non-mechanical generators and refrigerators. Presently, the use of thermoelectric devices is limited by the low thermo-electric conversion efficiency (Vining 2001). The efficiency of a refrigerator is expressed by the coefficient of performance (COP), which is the amount of cooling divided by the electrical energy input needed to obtain that cooling (DiSalvo 2009). The laws of thermodynamics tell that the maximum efficiency, called the Carnot efficiency, cannot be exceeded. The COP at Carnot efficiency is just $T_{cold}/(T_{hot} - T_{cold})$, where T_{hot} and T_{cold} are the temperatures of the ambient environment and the coldest part of the refrigerator, respectively. Present thermoelectric devices operate at about 10% of Carnot efficiency. The efficiency of a thermo-electric device is primarily determined by the materials used in the device. The performance of these materials depends on the Seebeck coefficient, α [μV K^{-1}], the electrical resistivity, ρ [μΩ m], and the thermal conductivity, λ [W K^{-1} m^{-1}], and is expressed in its figure-of-merit, *ZT*, which is given by $ZT = \alpha^2/(\rho\lambda)$ (Min et al. 1999). Thermoelectric materials are ranked by its figure-of-merit, *ZT*. A high value for *ZT* is a pre-requisite to be competitive compared with conventional refrigerators and generators (Majumdar 2004) (preferably near or even higher than the unity). A high-performance thermoelectric material is a semiconductor with the Seebeck coefficient and electrical resistivity decreasing with increasing doping concentration,

whereas the thermal conductivity increases with doping concentration (for p- and n-type materials) (Wijngaards et al. 2005). Typically, maximum thermoelectric performance is obtained at a doping concentration of about $n = 10^{19}$ cm^{-3} (Majumdar 2004). A generic thermoelectric component is basically composed of two strips of two different thermoelectric materials, or the same n- and p-doped, and electrically connected in series using a metal to avoid a pn junction (Wijngaards et al. 2005).

Conventional thermoelectric cooling materials are bulk solid solution alloys of Bi_2Te_3, Bi_2Se_3, and Sb_2Te_3, with the best materials having the best known values of ZT at room temperatures (Wijngaards and Wolffenbuttel 2005). In fact, these materials were developed in the early 1960s (Sales et al. 1996) and have found application in conventional bulk-sized converters due to their high Seebeck coefficient, low electrical resistivity and low thermal conductivity (Venkatasubramanian et al. 2001). The techniques used in the fabrication of telluride alloys-based bulk-sized thermoelectric converters can not be applied to fabricate the microcooler array presented in this paper, due to its reduced dimensions and the need of fabrication processes compatible with microsystem techniques. Alternatively, thin-films planar technology is the most suitable way to fabricate microconverters, due to the availability of large number of different types of substrate and the possibility to use the photolithographic techniques used in silicon IC technology (da Silva et al. 2002).

Different deposition techniques were tried to obtain thin-films of n-type bismuth telluride, Bi_2Te_3 and p-type antimony telluride, Sb_2Te_3. The experiments done by Da Silva have proven the impossibility to use the direct evaporation of the bulk materials to perform the deposition of Bi_2Te_3 thin-films (da Silva et al. 2002). The explanation was found in the large differences in vapour pressure of bismuth and tellurium that have resulted in a compositional gradient along the film thickness. Other techniques for the deposition of thin-films include the thermal co-evaporation (Helin et al. 2002), direct current (DC) magnetron sputtering (Bourgault et al. 2008), radio-frequency (RF) magnetron sputtering (Huang et al. 2009), electrochemical deposition (Lim et al. 2009), flash evaporation (Takachiri et al. 2008) and metal organic chemical vapour deposition (MOCVD) (Giani et al. 1999). Although all these approaches are in principle suitable, it was used the co-evaporation in this work to obtain both n-type Bi_2Te_3 and p-type Sb_2Te_3 thin-films, because it allows to precisely control the estequiometry of the deposited thin-film with lowest costs. Only MOCVD is better than co-evaporation to obtain thin-films with good uniformity and of the desired composition. However, thin film depositions using MOCVD require a reactor chamber and gases, whose toxicity can be dangerous to the human operators. Thus, high safety procedures are mandatory to follow. Moreover, the higher complexity of MOCVD makes it more expensive than co-evaporation (Lia et al. 2009).

3 Design and simulation of microcoolers array

Transversal (off-plane or vertical) and lateral (in-plane) approaches can be used for on-chip integration of thermoelectric devices, depending on the direction in which the heat is to be transported, relative to the surface of the device. For the microcooler array presented in this work, the lateral heat flow approach is implemented, because of its easier fabrication process and compliance with planar technology used in standard microelectronic processes (Tang et al. 2001).

As illustrated in Fig. 1, the solid-state array of microcoolers can accommodate up to 64 independent pixels organised in an 8 × 8 array structure. Electronics of control fabricated in a standard CMOS process will allow each pixel to be independently and digitally controlled to heat or cool. Figure 2 represents a single pixel cross-section, and when a current flows from the n-type thermoelectric element to the metal cold pad and from this to the p-type element, the Peltier effect avoids the heat absorption in the regions at the metal part and at the other end of the thermoelectric elements. Since electrical current flows to yield a heat flow, the Peltier effect causes heat generation at any resistive part in the circuit, including regions formed by the contact pads used to connect to electronic circuits.

Finite Element Modeling (FEM)-based simulations were performed to get an estimate of the expected temperature drop at each pixel. As depicted in Fig. 3, FEM simulations revealed a temperature drop of about 15°C, below room

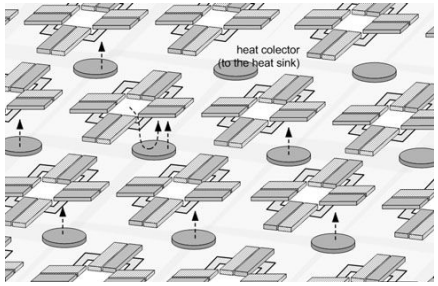

Fig. 1 An artist impression showing a part of the microcoolers array. In this artwork, the heat is collected by each pixel (constituted by 4 thermoelectric n-/p-type material pairs) on bottom of the supporting membrane and directed to the heat collectors (on top of the supporting membrane), to be dissipated in a heat sink (the heat flow from the bottom to the top is represented with *dashed lines* and *arrows*)

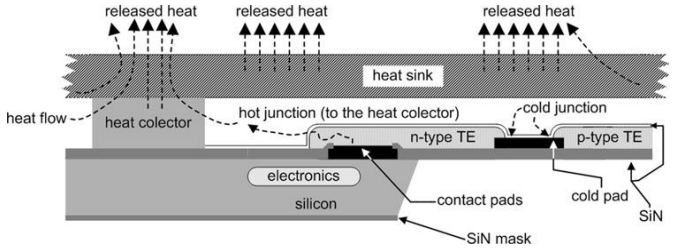

Fig. 2 Artwork of a pixel in the microcooler array (not drawn on scale), where it can be observed the heat flow path

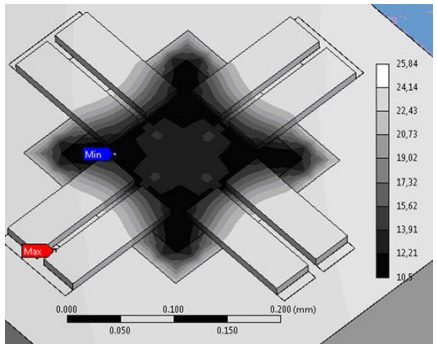

Fig. 3 The simulations performed on a single microcooler pixel to demonstrate the possibility of a 15°C temperature drop at the centre of the pixel

temperature. A silicon nitride membrane with a thickness of 200 nm supports four pairs of microcooler elements measuring 40 μm × 100 μm × 10 μm and absorbing a total current supply of 14 mA.

In the simulations a contact resistivity between the metal pads and thermoelectric elements of 10^{-10} Ωm^{-2} was assumed (da Silva and Kaviany 2004; Birkholz et al. 1987). A heat flow due to radiation and convection from the cooled surface of 10 W m^{-2} K^{-1} was included in the simulations. The simulations were based on the thermoelectric properties for n- and p-type Bi_2Te_3/Sb_2Te_3 elements measured by Gonçalves et al. (2006a, b) and listed in Table 1. The results obtained from the finite elements method simulations on a single microcooler's pixel showed an agreement of those and with theoretical calculations (Völklein et al. 1999).

The cold junctions of all 64 Peltier microcoolers are on a silicon nitride (Si_3Ni_4) membrane, whereas the hot junctions and the support electronics are positioned on top of the silicon wafer, as shown in Fig. 4. The heat generated by circuits and by thermoelectric elements is distributed over the silicon wafer removed using a heat-sink glued around the microchip. The overall expected effect of this self-heating on the temperature profile of the backside of the microchip due to the control electronics, Peltier effect and Joule heating is shown in Fig. 4. Two assumptions were made with respect to self-heating: Firstly, the power consumption in the electronics controlling each pixel is 1 mW. Secondly, a current of 14 mA is supplied to each microcooler. A fixed temperature of 25°C was imposed at the outer edge of the array (where the heat-sink is located) for a silicon wafer with a thickness of 500-μm. At these conditions a temperature of 27.4°C was observed at the backside of the silicon wafer.

An integrated circuit was designed in a CMOS process for addressing and controlling each pixel in the microcooler array, as well as to monitor their state. Figure 5a shows the block diagram of the microcooler array, where for simplification purposes only a 2 × 2 subset is presented. The projection of Fig. 5b is a full schematic of a power circuit that drives each pixel in the microcooler array. This circuits uses rectangular pulses to control the power supplied to each pixel and thus, to adjust the cooling settings of that particular pixel. The power is adjusted by changing the duty-cycle of the input signal in such a way that the voltage across the input capacitor increases in time in case of a duty cycle larger than 50%, whereas this voltage decreases in time for duty-cycles smaller than 50%. The voltages between the gate and the source of MOSFETs Q_1 and Q_2 increase and decrease, respectively, when the voltage in the capacitor is positive. This makes the current in Q_1 to increase and the current in Q_2 to decrease. The inverse mechanism is implemented using the voltage gate-source and the current in Q_1 and Q_2. When the voltage across the input capacitor decreases. MOSFETs Q_5 and Q_4 are used for biasing MOSFETs Q_1 and Q_2. The power applied to each pixel is easily controlled with this circuit. The supply voltages (at nodes V_{dd} and V_{ss}) and the dimensions of MOSFETs Q_1 and Q_2 must be designed to supply the maximum current (14 mA) to the microcooler array with MOSFETs Q_1 and Q_2 kept in the triode region to minimize power dissipation. Operating these MOSFETs in

Table 1 The most important thermoelectric propoerties of selected thin-films (TFs) measured at room temperature (300 K ≈ 27°C)

TF	Te (%)	α (V K^{-1})	ρ (Ωm)	λ (W m^{-1} K^{-1})	n (cm^{-1})	PF (W K^{-1}m^{-2})	ZT at 300 K
Sb_2Te_3	30	188 × 10^{-6}	12.6 × 10^{-6}	1.7	1–7 × 10^{19}	3.62 × 10^{-3}	0.50
Bi_2Te_3	38	−248 × 10^{-6}	17 × 10^{-6}	1.3	3–20 × 10^{19}	2.81 × 10^{-3}	0.84

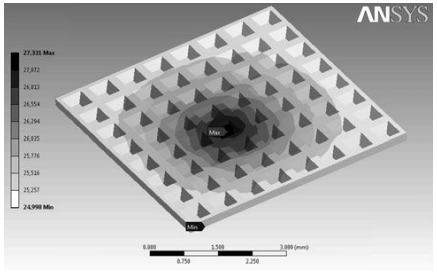

Fig. 4 The simulated temperature profile over the backside of the structure in case of maximum cooling power applied to all pixels

the saturation region is for this reason not desirable, especially when many pixels are switched on. The dissipation results in device heating and consequently in an increased substrate temperature.

4 Fabrication

The sequence of fabrication steps applied for realization of the microcooler array is presented in Fig. 6. The backside of the wafer is covered with a patterned silicon nitride layer, which is used as mask during etching in the final fabrication step. The silicon wafer containing the fabricated electronics is also covered with a layer of nitride silicon on top. Two vias are opened on top layer, in order to use the available contact metallic pads to connect thermoelectric elements to external circuits. Also, this silicon nitride layer is used to fabricate the membrane needed to support the coolers, where the areas of reduced temperature are located. The next step is the deposition and patterning of metal pads to provide interconnection between thermoelectric elements. The p-type Sb_2Te_3 material is deposited by co-evaporation and patterned by photolithography done on top of the wafer. An aqueous solution composed by 10:6:26 HNO_3:HCl:H_2O (99.5% HNO_3 and 37% HCl) etches the Sb_2Te_3 p-type thin-film and keeps unchanged the metal contact pads without etching (da Silva and Kaviany 2005). Moreover, the etch-rate on metal pads was measured to be below 0.1 nm s^{-1}.

The co-evaporation method is also used to do the depositions of the n-type Bi_2Te_3 material; the same applies to the patterning method. Figure 7a, b are cross-sectional SEM photographs of deposited (and selected) p- and n-type Sb_2Te_3/Bi_2Te_3 thin-films (TFs), respectively, whose thermoelectric properties are listed in Table 1. A selectivity of 50:1 is obtained with HNO_3 (30% diluted in water) with etch-rates of 250 and 5 nm s^{-1} for Sb_2Te_3 and Bi_2Te_3

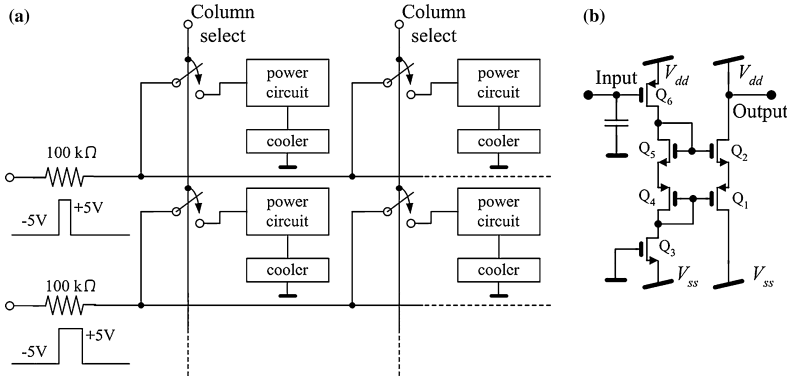

Fig. 5 **a** Block diagram showing a 2 × 2 subpart of the microcooler array, and **b** the schematic of power circuits that drives each of the 64 pixels in the microcoolers array

Fig. 6 The fabrication steps for the microcooler array

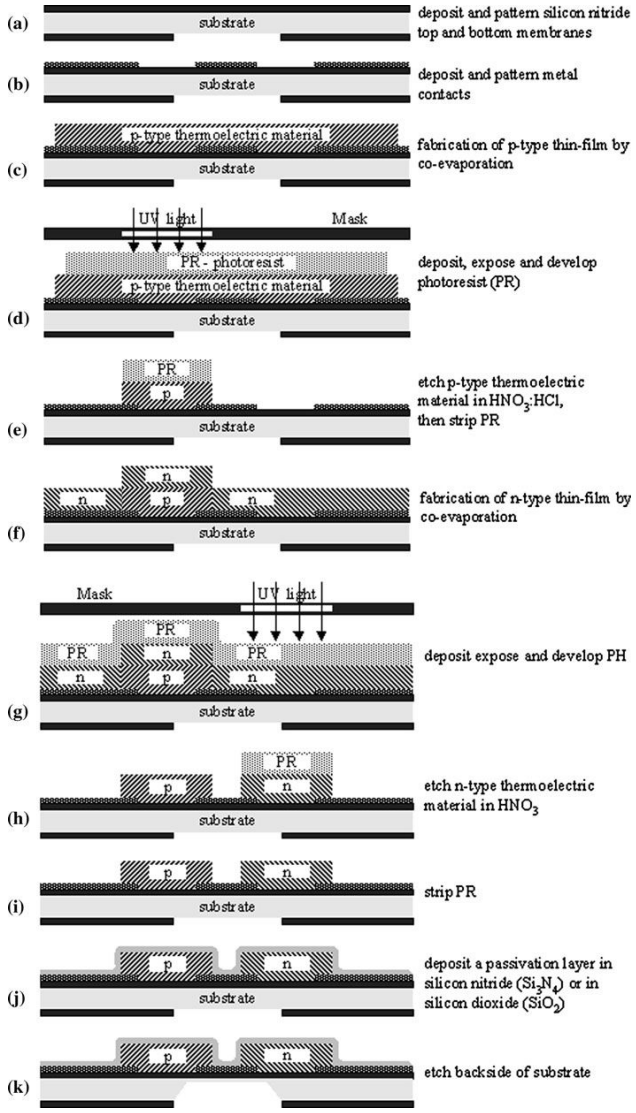

thin-films, respectively (da Silva and Kaviany 2005). It should be noted that the etch-rate measurements were done for all p- and n-type thin-films deposited on 25 μm-thick polyimide (kapton) substrates. A silicon nitride passivation layer is applied after removal of the photoresist, in order to avoid degradation of thermo-electric thin-films by contact

with atmospheric oxygen. Finally, the back side of the silicon wafer is etched in an alkaline solution of potassium hydroxide (KOH), in order to fabricate the silicon nitride membrane to support the different pixels of the microcoolers array. This membrane needs to be poorly thermally conductive to minimize reverse heat leakage between the hot and the cold side of the Peltier microcoolers. The electronic circuits must be protected during the potassium hydroxide etching and must for this reason be located in the regions between the microcoolers.

5 Experimental results

Figure 8 shows an enlarged version of the microcoolers array with four pairs of thermoelectric elements, which was fabricated to validate the feasibility of the solid-state cooling probe concept. The design of the enlarged microcooler pixel avoids some of the fabrication issues presently investigated, while it enables the analysis of the performance of the thermoelectric materials used and demonstrates basic operation of the microcooler. An infrared microscope was used to acquire thermal image maps, which enables an assessment of the performance of the microcooler. Figure 9 illustrates the measurement setup used for thermal image acquisition with the help of an infrared microscope. The background temperature was set at 50°C to enhance image sensitivity by heating the device inside the chamber and the chamber.

Figure 10 shows a thermal image obtained with a current of 4 mA flowing through the device. A first qualitative inspection allows immediate identification of the cold and hot regions of the surface. The temperature profiles along the A–A′ and B–B′ lines in Fig. 10 are the lines across the p- and n-type elements and are shown in Fig. 11. The high contact resistances between thermoelectric elements and metal pads resulted in a maximum measured temperature

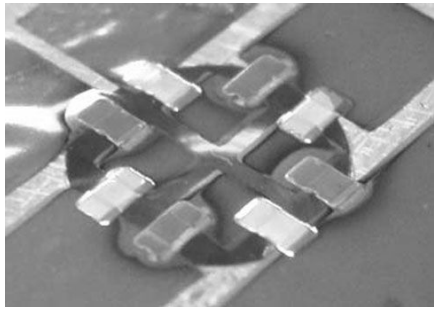

Fig. 8 An enlarged version of the microcoolers array with four pairs of planar thermoelectric elements

difference of only 5°C in vacuum between the cold and the hot sides.

The contact resistance was measured using the procedure proposed by Gonçalves et al. 2006a, b, which is based on transmission line method. This method resulted in the measurement of a contact resistance of 10^{-6} Ωm^2. A reduction in the contact resistance will be expected (increasing the temperature difference between the cold and the hot sides) to less than 10^{-9} Ωm^2 by using an interface layer in the fabrication process (da Silva and Kaviany 2005).

Also, it must be noted that the high temperature achieved on the hot side of the device results from the low dissipation capability due to the low thermal conductivity of the substrate used in the prototype (polyimide) compared with the substrate used in simulation (silicon covered with silicon nitride). The higher temperature observed on the hot side of the device is also due to the low thermal conductivity at the contact pads. Relatively straightforward

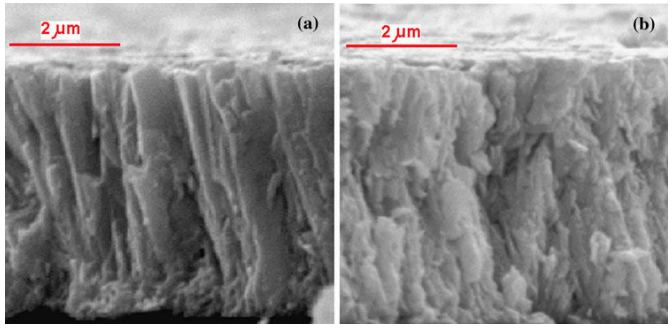

Fig. 7 Cross-section SEM photographs of the deposited, **a** p- and **b** n-type Sb_2Te_3/Bi_2Te_3 thin-films

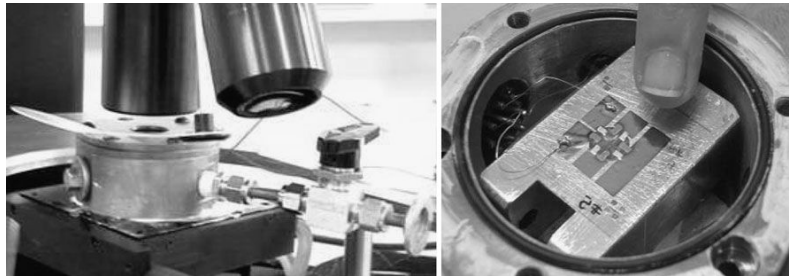

Fig. 9 Measurement setup for the acquisition of thermal images

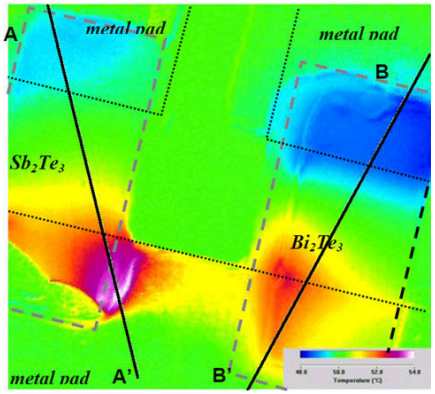

Fig. 10 An acquired thermal image of p- and n-type thermoelectric elements in vacuum powered with a current of 4 mA

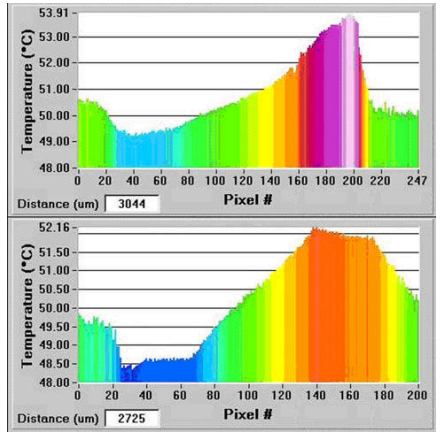

Fig. 11 Thermal profiles along the lines (*top*) A–A′ and (*bottom*) B–B′, obtained on sections of p- and n-type elements, respectively

changes in design and fabrication can be implemented to significantly improve performance.

6 Conclusions

This paper presents the design, simulation and fabrication process of a microcoolers array composed by 64 pixels and an electronic system—in CMOS—to independently control the cooling rate at each pixel. The simulations demonstrate the capability for a temperature difference up to ±15°C.

Sb_2Te_3 and Bi_2Te_3 are thermoelectric materials of p- and n-type, respectively, and thin-films of both materials were successfully obtained by co-evaporation. This deposition method showed the suitability for fabrication of microcooler arrays. Photolithography was also successfully applied for definition of the thin-films based on Bi_2Te_3 and Sb_2Te_3. These materials were patterned with 3:7 HNO_3:H_2O and 10:6:26 HNO_3:HCl:H_2O (99.5% HNO_3 and 37% HCl), respectively. A selectivity of 50:1 was measured between these two processes. Using this fabrication technique an enlarged version of a single pixel of the microcooler was fabricated and its performance, as analyzed using a microscopic infrared imaging system, demonstrate the cooling concept. However, the measurements showed an achievable maximum temperature difference of only 5°C. The explanations on observed differences from the expected performance are due to high electrical resistance and low thermal conductance obtained at the interface between the thermoelectric material and the metal pad. Significant improvements are well possible by an improved technology. Moreover, a larger temperature step is possible, at the expense of efficiency, using

several cascaded thermo-electric elements thermally in series between the area to be cooled and ambient.

The results obtained for the deposited thin-films based on tellurium alloys (Sb_2Te_3/Bi_2Te_3) and the fabricated initial prototype of a microcooler pixel demonstrates the feasibility of the probe with a solid-state 64-element microcooler array. The main application is as a medical instrument, since cooling-probes can locally cool the human tissue to temperatures of 25°C and temporarily stop bleedings.

Acknowledgments This work was fully supported by FCT/PTDC/EEA-ENE/66855/2006 project.

References

Altshuler GB, Zenzie HH, Erofeev AV, Smirnov MZ, Anderson RR, Dietrickx C (1999) Contact cooling of the skin. Phys Med Biol 44:1003–1023

Anvari B, Milner TE, Tanenbaum BS, Kimel S, Svaasand LO, Nelson JS (1995) Selective cooling of biological tissues: application of thermally mediated therapeutic procedures. Phys Med Biol 40:241–252

Argonne National Laboratory (2006) Rapid cooling technology could aid surgery patitents, heart attack victims. The University of Chicago, Argonne National Laboratory, Public Note, p 1

Bell L (2008) Cooling, heating, generating power, and recovering waste heat with thermoelectric systems. Science 321:1457–1461

Birkholz U, Fetting R, Rosenzweig J (1987) Fast semiconductor thermoelectric devices", Sens. Actuators A 12:179–184

Bourgault D, Garampon C, Caillault N, Carbone L, Aymami JA (2008) Thermoelectric properties of n type $Bi_2Te_{2.7}Se_{0.3}$ and p-type $Bi_{0.5}Sb_{1.5}Te_3$ thin films deposited by direct current magnetron sputtering. Thin Solid Films 516:8579–8583

Cheung EH, Arcidi JM Jr, Jackson ER, Hatcher CR Jr, Guyton RA (1988) Intracavitary right heart cooling during coronary bypass surgery. Circulation 78:173–179

da Silva LW, Kaviany M (2004) Micro-thermoelectric cooler: interfacial effects on thermal and electrical transport. Int J Heat Mass Transfer 47:2417–2435

da Silva LW, Kaviany M (2005) Fabrication and measured performance of a first-generation microthermoelectric cooler. J Microelectromech Syst 14:1110–1117

da Silva LW, Massoud K (2002) Miniaturized thermoelectric cooler. In: Proceedings of the IMECE'02, New Orleans, pp 154–161

Davidson SRH, Sherar MD (2003) Theoretical modelling, experimental studies and clinical simulations of urethral cooling catheters for use during prostate thermal therapy. Phys Med Biol 48:729–744

DiSalvo FJ (2009) Thermoelectric cooling and power generation. Science 285:703–706

DORC (2011) Dutch ophthalmic research center international BV. http://www.dorc.nl/. Accessed 13 May 2011

Giani A, Boulouz A, Delannoy FP, Foucaran A, Charles E, Boyer A (1999) Growth of Bi_2Te_3 and Sb_2Te_3 thin films by MOCVD. Materials Sci Eng B 64:19–24

Gonçalves LM, Couto C, Alpuim P, Correia JH (2006a) Optimization of thermoelectric thin-films deposited by coevaporation on plastic substrates. In: Proceedings of the ECT'06, Cardiff

Gonçalves LM, Couto C, Alpuim P, Correia JH (2006b) Flexible thin-film planar Peltier microcooler. In: Proceedings of the ICT'06, Vienna

Haugk M, Sterz F, Grassberger M, Uray T, Kliegel A, Janata A, Richeling N, Herkner N, Laggner AN (2007) Feasibility and efficacy of a new non-invasive surface cooling device in post-resuscitation intensive care medicine. Resuscitation 75:76–81

Helin Z, Rowe DM, Williams SGK (2002) Peltier effect in a co-evaporated Sb_2Te_3(P) Bi_2Te_3(N) thin films thermocouple. Thin Solid Films 408:270–274

Huang H, Luan W, Tu S (2009) Influence of annealing on thermoelectric properties of bismuth telluride films grown via radio frequency magnetron sputtering. Thin Solid Films 517:3731–3734

Larin KV, Larina IV, Motamedi M, Esenaliev RO (2002) Optoacoustic laser monitoring of cooling and freezing of tissues. Quantum Electr 32:953–958

Lewis G, Mackenzie A (1971) Cooling during major vascular surgery. Br J Anaesth 44:859–864

Lia ZM, Hao Y, Zhanga JC, Yanga LA, Xua SR, Changa YM, Bia ZW, Zhoua XW, Nia JY (2009) Thermal transportation simulation of a susceptor structure with ring groove for the vertical MOCVD reactor. J Crystal Growth 311:4679–4684

Lim S, Lim M, Oh T (2009) Thermoelectric properties of the bismuth-antimony-telluride and the antimony-telluride films processed by electrodeposition for micro-device applications. Thin Solid Films 517:4199–4203

Majumdar A (2004) Thermoelectricity in semiconductor nanostructures. Science 303:777–778

Min G, Rowe DM (1999) Cooling performance of integrated thermoelectric microcooler. Solid-State Electronics 43:923–929

Sales BC, Mandrus D, Williams RK (1996) Filled skutterudite antimonides: a new class of thermoelectric materials. Science 272:1325–1328

Takachiri M, Miyazaki K, Tsukamoto H (2008) Structural and thermoelectric properties of fine grained $Bi_{0.4}Te_{3.0}Sb_{1.6}$ thin-films preferred orientation deposited by flash evaporation method. Thin Solid Films 516:6336–6343

Tang K, Man KF, Chen G, Kwon S (2001) An optional fuzzy PID controller. IEEE Trans Ind Electron 48:757–761

Treasure T (1988) Hypothermic protection (26 degrees-25 degrees C) without perfusion cooling for surgery of congenital cardiac defects using prolonged occlusion. Thorax Int J Respir Med 43:945

Venkatasubramanian R, Silvola E, Colpits T, O'Quinn B (2001) Thin-film thermoelectric devices with high room-temperature figures of merit. Nature 413:597–602

Vining CB (2001) Semiconductors are cool. Nature 413:577–578

Völklein F, Min G, Rowe DM (1999) Modeling of a microelectromechanical thermoelectric cooler. Sens Actuators A 75:95–101

Wijngaards DDL, Wolffenbuttel RF (2005) Thermo-electric characterization of APCVD $PolySi_{0.7}Ge_{0.3}$ for IC-compatible fabrication of integrated lateral Peltier elements. IEEE Trans Electr Dev 52:1014–1025